Neutrosophic set with Adaptive Neuro-Fuzzy Inference System for Liver Tumor Segmentation and Classification Model

Mohammed I. Alghamdi

Department of Computer Science, Al-Baha University, Al-Baha City, Kingdom of Saudi Arabia

Email: mialmushilah@bu.edu.sa

Abstract

Lung cancer is the abnormal development of cells in the lung causes serious risk to the health since lung has an interconnected system of blood vessel and lymphatic channel exposed to metastasis. The survival rate of lung cancer depends greatly on the earlier diagnosis and staging of the lung cancer. Computed Tomography (CT) image is commonly employed for lung cancer diagnosis since they offer data regarding distinct portions of the lung. The exactness of finding tumor location, volume and shape acting a major role in positive treatment and diagnosis of tumor. This article designs a novel neutrosophic set with adaptive neuro-fuzzy inference system for liver tumor segmentation and classification (NSANFIS-LTSC) model. The presented NSANFIS-LTSC model aims to identify and classify the presence of liver tumor from medical images. The presented NSANFIS-LTSC model primarily undergoes pre-processing to eradicate the noise. Followed by, the neutrosophic set (NS) based segmentation is applied to identify the affected tumor regions in the CT images. Besides, DenseNet-169 model is utilized to create feature vectors and dragonfly algorithm (DFA) is applied to tune the hyper parameters of the DenseNet-169 model. Finally, ANFIS classifier is exploited for the occurrence and classification of liver tumor. The simulation analysis of the NSANFIS-LTSC model is experimented using benchmark dataset and the results are investigated under several aspects. The simulation outcome reported the betterment of the NSANFIS-LTSC model over the recent methodologies.

Keywords: Liver tumor, Image segmentation, Medical imaging, Deep learning, Disease classification

1. Introduction

Liver cancer is quite possibly the most well-known kinds of cancerous illness around the world, with progressively high dismalness [1]. Early conclusion and therapy are critical to further develop the endurance rate, and the clinical imaging methods give incredible assistance [2]. Computed Tomography (CT) is broadly utilized for analysis of hepatic illness as it can furnish generally high goal pictures with precise physical data. Effective segmentation of cancer from CT pictures is a significant essential for early conclusion, therapy arranging, and checking of liver cancer. Be that as it may, manual segmentation of liver tumors cut by cut is still regularly involved by radiologist, which is difficult and tedious because of the huge measure of information, and furthermore inclined to interobserver inconstancy [3, 4]. The requirement for precise and effective tumor depiction prompts the improvement of self-loader or programmed tumor segmentation strategies. CT scans offer itemized cross sectional pictures of the stomach district. More often than not further handling of these stomach CT scan pictures is expected for segmenting the healthy and affected regions from the remainder of the CT picture substance. Yet at the same time, the power likeness between the tumor and other close by tissues in the CT pictures made the

DOI: https://doi.org/10.54216/IJNS.180202

Received: November 08, 2021 Accepted: March 02, 2022

segmentation of the tumorous regions too troublesome. Consequently, these pictures should be handled and improved to separate the cancerous tissue. In a CT scan, the presence of liver cancer can be distinguished by the distinction in pixel power in contrast with the encompassing solid liver, for example the tumor region might be more obscure (hypodense) or more splendid (hyperdense) than the encompassing solid liver [5].

Classification of hepatic malignancy relies upon the size and area of the tumor [6]. Thus, it is vital to foster a programmed technique to distinguish and extricate the cancer district from the CT scan precisely. Picture segmentation is the most common way of apportioning the liver district in the CT scan into locales, where every area addresses a semantic piece of the liver [7]. This is a principal step to help the determination by radiologist, and a crucial stage to make programmed PC supported conclusion (CAD) frameworks [8]. CT scan is generally deciphered by manual or semi-manual procedures, however these methods are emotional, costly, tedious, and profoundly blunder inclined. To conquer these snags and work on the nature of liver tumor determination, various PC helped strategies have been created. In prior days, different conventional methods were utilized to separate tumors from liver pictures [9]. In any case, these strategies were not completely viable in the extraction of the tumor. A large portion of them are manual or self-loader and ward tense identifiers instead of investigating the picture as a pixel. An assortment of deep-learning techniques have likewise been produced for programmed or self-loader segmentation of liver tumors [10].

Xu et al. [11] proposed a new PA-ResSeg model for designing multiple phase features to accurately segment the liver tumor. A phase attention (PA) is presented for extra exploitation of the images to assist segmentation outcomes. It allows leanring highly defined multi-phase features based on the channel dependency and recalibration of the ART features using the learnt interdependency among the phases. Chlebus et al. [12] developed a completely automated segmanttion model for liver cancer using DL model with object based post-processing stage. The presented model is experimented and the results are inspected under distinct ways. Deng et al. [13] generalized a procedure of level set with new model of adaptive regulation to energy functional parameter. It is completely automated when the tumor region is identified. Zheng et al. [14] presented a model to segment liver and liver tumor regions. It is based on level set model (LSM) integrating region as well as edge details. It is highly resistive to the edge leakages compared to single-information driven LSM to segment liver.

This article designs a novel neutrosophic set with adaptive neuro-fuzzy inference system for liver tumor segmentation and classification (NSANFIS-LTSC) model. The presented NSANFIS-LTSC model aims to identify and classify the presence of liver tumor from medical images. The presented NSANFIS-LTSC model primarily undergoes pre-processing to eradicate the noise. Followed by, the neutrosophic set (NS) based segmentation is applied to identify the affected tumor regions in the CT images. Besides, DenseNet-169 model is utilized to create feature vectors and dragonfly algorithm (DFA) is applied to tune the hyper parameters of the DenseNet-169 model. Finally, ANFIS classifier is exploited for the occurrence and classification of liver tumor. The simulation analysis of the NSANFIS-LTSC model is experimented using benchmark dataset and the results are investigated under several aspects.

2. Design of Liver Tumor Segmentation and Classification Model

This article has developed a new NSANFIS-LTSC to identify and classify the presence of liver tumor from medical images. The presented NSANFIS-LTSC model mainly undergoes pre-processing to eliminate the noise. In addition, NS based segmentation is applied to identify the affected tumor regions in the CT images. Moreover, DFA with DenseNet-169 model is utilized to create feature vectors and ANFIS classifier is exploited for the occurrence and classification of liver tumor. Fig. 1 shows the workflow of projected technique.

DOI: https://doi.org/10.54216/IJNS.180202

Received: November 08, 2021 Accepted: March 02, 2022

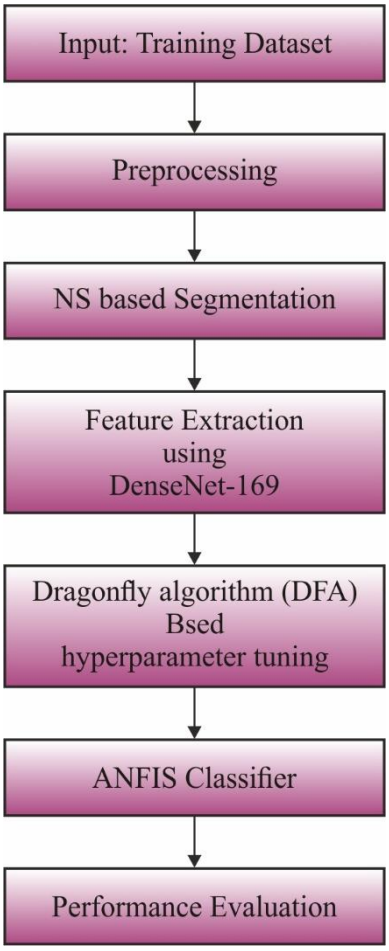

Fig. 1. Workflow of NSANFIS-LTSC model

2.1 NS based Segmentation

The presented method is a subdivision of philosophy, it is a generality of fuzzy set, intuitionistic set, dialetheist set, para-consistent set, tautological set, and a paradoxist set. Neutrosophic set and its features are briefly deliberated in [15]. The problem that could not resolved through fuzzy logic is addressed through neutrosophic logic. This is due to NS presents novel module named indeterminacy and analyses the neutrosophic logical value of the proposition that characterized as follows.

Definition l (Neutrosophicset). Consider T, I, and F represent neutrosophic component. Where T, I, and F denotes normal or non-normal real subset of $]^{-}0, 1^{+}[$. A component $A(T, I, F)$ belonging to the established manner: it is f false ($f \in F$) , t true ($t \in T$), and i indeterminate ($i \in I$) , whereas t, i, and f denotes the real number.

For applying neutrosophy, image should be transported to a neutrosophic field P_{NS}. A pixel in the neutrosophic field is characterized by T, I, and F which implies the pixel is i% indeterminate, f% false, and t% true, whereas f differs in F, t differs in T, and i differs in I, correspondingly. In neutrosophic set, $0 \leq t, i, f \leq 1$. But, in a traditional set, $i = 0$, t and f is 0 or 1 and in a fuzzy set, $i = 0{,}0 \leq t, f \leq 1$[33]. Fig. 1 displays the relations among a neutrosophic and additional sets.

$T(i,j)$, $I(i,j)$, $F(i,j)$ denotes the neutrosophic set mechanisms, all the pixels $P(i,j)$ in image field transmuted to NS field $P_{NS}(i,j)$ in the following:

$$P_{NS}(i,j) = \{T(i,j), I(i,j), F(i,j)\} \quad (1)$$

DOI: https://doi.org/10.54216/IJNS.180202

Received: November 08, 2021 Accepted: March 02, 2022

$$T(i,j) = \frac{g(\bar{i},j) - \overline{g}_{min}}{\overline{g} - \overline{g}_{min}} \quad (2)$$

$$I(i,j) = 1 - \frac{Ho(i,j) - \overline{Ho}_{\min}}{\overline{Ho}_{\max} - \overline{Ho}_{miI}} \quad (3)$$

$$F(i,j) = 1 - T(i,j) \quad (4)$$

$$Ho(i,j) = abs(g(i,j) - g(\bar{i},j) \quad (5)$$

Whereas $Ho(i,j)$ represent the homogeneity value and $g(\bar{i},j)$ denotes the local mean value of window size.

Definition 2 (Neutrosophy image entropy). It can be determined as the sum of three subset entropies , F, and T. When the entropy is maximal, the dissimilar intensities have equivalent possibility and the intensity distributes regularly. When the entropy is smaller, the intensity has divergent possibilities and the distribution is not uniform.

$$En_T = -\sum P_T(i) \ln P_T(i) \quad (6)$$

$$En_F = -\sum P_F(i) \ln P_F(i) \quad (7)$$

$$En_I = -\sum P_I(i) \ln p(i) \quad (8)$$

$$En_{NS} = En_T + En_I + En_F \quad (9)$$

Whereas En_I, En_T and En_F denotes the entropy of subset T, I and F, correspondingly. $P_T(i)$, $P_F(i)$, and $P,(i)$ indicates the probability of component i in T, I and F. En_I, is applied for evaluating the dispersal of indeterminacy, and En_T and En_F are employed for measuring the dispersal of the components in NS.

2.2 Feature Extraction

After tumor segmentation, DenseNet-169 model is utilized to create feature vectors [16]. DenseNet (Dense Convolutional Network) is a structure that focused on creating the deep learning network goes deeper, however makes them very effective to training simultaneously, through short interconnection amongst the layers. DenseNet-169 was selected as depth of 169 layers it is quite lower in parameter than other methods, and the structure manages the vanishing gradient problems. In the DenseNet-169 structure the final fully connected (FC) layer was removed, in its defect, a 256 class FC layers was formed, a 128 class FLC and ten node FLC using softmax activation for the output. However, last layer employed ReLU activation function.

Besides, the DFA is applied to tune the hyper parameters of the DenseNet-169 model. DFA is primarily changed from static and dynamic presentations of dragonfly swarming performance [17]. In DFA, 3 swarming behaviors are determined below:

- Separation: It implies the removal of individual static collision from others.
- Alignment: It implies the individual velocity correspond to alternative neighbouring separate.
- Cohesion: It denotes individual ability to neighboring mass centre.

Survival rate is the primary objective of swarm whereby every individual is externally disturbed and fascinated toward the direction of food. Due to this actions, 5 significant characteristics influence the individual upgrade position are Alignment, Separation, Attraction, Cohesion to food direction, and Distraction of enemy. This characteristics are arithmetically described in the following.

Separation: it can be estimated by the Eq (10):

DOI: https://doi.org/10.54216/IJNS.180202

Received: November 08, 2021 Accepted: March 02, 2022

$$S_i = -\sum_{k=1}^{M} Y - Y_k, \tag{10}$$

Whereas Y denotes the individual existing location, Y_k indicates the position of *k-th* neighborhood individuals and M determines the entire amount of neighborhood separations.

Alignment: It displays the mean of velocity that is defined as follows:

$$A_i = \frac{\sum_{k=1}^{M} V_k}{M}, \tag{11}$$

Whereas $V_k$indicates the velocity of *k-th* neighborhood individual.

Cohesion: it can be estimated by the following:

$$C_i = \frac{\sum_{k=1}^{M} Y_k}{M} - Y \tag{12}$$

Attraction towards a food source: It indicates distances amongst position of existing individuals and setting of food direction (Y^+) and it is defined as follows:

$$F_i = Y^+ - Y \tag{13}$$

Distraction outwards an enemy: It implies distances amongst location of existing individuals and location of enemy (Y^-) is estimated by Eq (14):

$$E_i = Y^- - Y \tag{14}$$

In dragonfly, nature is a unification of 5 parameters. Next, 2 vectors are applied to upgrade dragonfly position in a searching space, i.e., position vector (Y) and step vector $(\triangle Y)$. Step vector is demonstrated by Eq. (15):

$$\triangle Y_{t+1} = (aA_i + sS_i + cC_i + eE_i + fF_i) + w \triangle Y_t\,, \tag{15}$$

The individual location vector is demonstrated by:

$$Y_{t+1} = Y_t + \triangle Y_{t+1} \tag{16}$$

In the event of optimization model, dissimilar explorative and exploitative actions are achieved as 3 variables $(a, s, c, e,$ and $f)$. Also, this variable is applied in handling exploitation and exploration stages.

The dragonfly convergence can be guaranteed through the iteration of parameter weights viz. adapted consequently. Therefore, flying path of dragonfly is transformed as an optimization method is treated.

2.3 ANFIS Classification

At the final stage, the ANFIS classifier is exploited for the occurrence and classification of liver tumor [18]. ANFIS combines FIS and ANN. ANFIS doesn't have the limitation of ANN and FIS, namely sensitivity and overfitting to define membership function. Therefore, it effectively implements in prediction problem. The popular technique method to train ANFIS is the Sugeno-type FIS, that employs a strong learning method for determining the parameter of the fuzzy scheme for training the model [19]. For two inputs (x1, x2) of Sugeno-type FIS depends on the {if-then} fuzzy rules, the output y of ANFIS is given by

$$Rule\ 1. If\ (x1\ is\ A1)\ and\ (x2\ is\ B1)\ then\ y1 = p1x1 + q1x2 + r1 \tag{17}$$

$$Rule\ 2. If\ (x2\ is\ A2) and\ (x2\ is\ B2) then\ y2 = p2x1 + q2x2 + r2 \tag{18}$$

DOI: https://doi.org/10.54216/IJNS.180202

Received: November 08, 2021 Accepted: March 02, 2022

Whereas A and B denotes fuzzy sets, and p, q, and r indicate model parameter that is defined in the trained phase. ANFIS model usually involves 5 layers. Initially, the input information passes over dissimilar membership functions, and the membership amount of input node to dissimilar fuzzy interludes can be defined by the membership function. It has different kinds of membership function, includes trapezoid, triangular, bell, and Gaussian functions. Gaussian function was utilized because it can be determined as mean and standard deviation. Next, it has the rule node, fuzzy value is multiplied with all the nodes, also the outcome is the weights of the rule. This layer employs the "AND" operator. The node of the 3rd layer normalizes the weight of the rule. The resulting node creates the fuzzy-based rule output. The 5th layer is the final layer, comprises of an individual node which estimates the overall output. This layer transmutes the outcomes of all the fuzzy rules into a non-fuzzy output through a defuzzification procedure. The structure of ANFIS model is shown in Fig. 2.

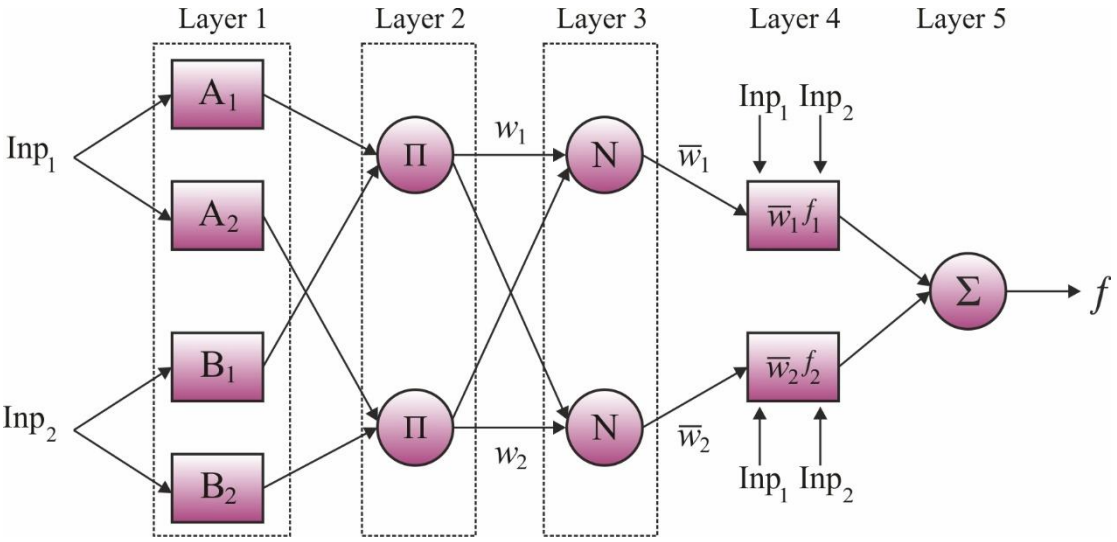

Fig. 2. Structure of ANFIS

3. Experimental Validation

This section inspects the experimental validation of the NSANFIS-LTSC model using benchmark CT images. Sample images are shown in Fig. 3. Table 1 provides a detailed outcomes of the NSANFIS-LTSC model and other models interms of Jaccard and Dice.

DOI: https://doi.org/10.54216/IJNS.180202

Received: November 08, 2021 Accepted: March 02, 2022

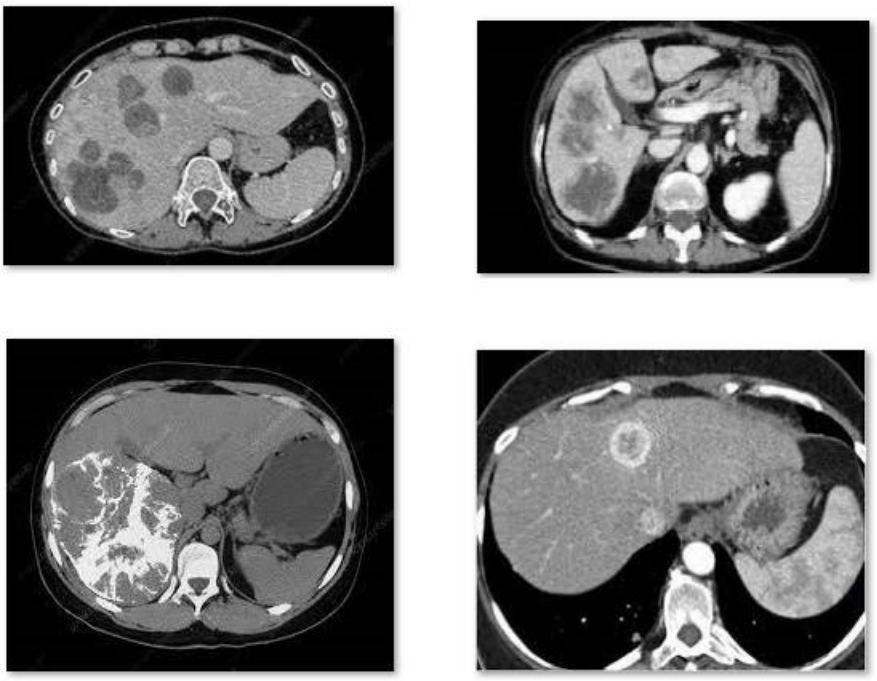

Fig. 3. Sample images

DOI: https://doi.org/10.54216/IJNS.180202

Received: November 08, 2021 Accepted: March 02, 2022

Table 1 Overall results of NSANFIS-LTSC model with other models

No. of Images	NSPSO-FCM		FFCM		PSO-FCM		NSANFIS-LTSC	
	Jaccard	Dice	Jaccard	Dice	Jaccard	Dice	Jaccard	Dice
Image-1	38.56	55.70	34.14	49.84	34.53	51.85	42.11	58.44
Image-2	36.68	53.13	32.44	48.41	31.84	49.76	40.59	56.13
Image-3	18.30	30.29	15.14	27.31	15.90	25.81	22.26	34.54
Image-4	38.44	55.97	32.05	48.68	34.13	51.98	41.75	58.89
Image-5	24.10	39.47	17.23	31.40	19.25	33.49	28.53	43.45
Image-6	37.69	56.09	35.27	51.10	36.12	51.95	40.45	59.15
Image-7	39.19	56.24	35.48	50.90	34.97	51.84	43.52	60.73
Image-8	38.54	54.52	29.85	46.97	33.29	49.14	41.97	58.98
Image-9	32.49	50.22	25.86	42.59	27.32	42.45	36.15	53.47
Image-10	23.81	40.45	19.70	31.79	19.64	32.94	27.88	43.58

Fig. 4 depicts the results obtained by the NSPSO-FCM model on ten distinct images. On applied image 1, the NSPSO-FCM model has offered Jaccard and Dice of 38.56% and 55.70%. Similarly, on applied image 2, the NSPSO-FCM model has provided Jaccard and Dice of 36.68% and 53.13%. Likewise, on applied image 3, the NSPSO-FCM model has achieved Jaccard and Dice of 18.30% and 30.29%. Moreover, on applied image 4, the NSPSO-FCM model has attained Jaccard and Dice of 38.44% and 55.97%. Finally, on applied image 10, the NSPSO-FCM model has resulted to Jaccard and Dice of 23.81% and 40.45%.

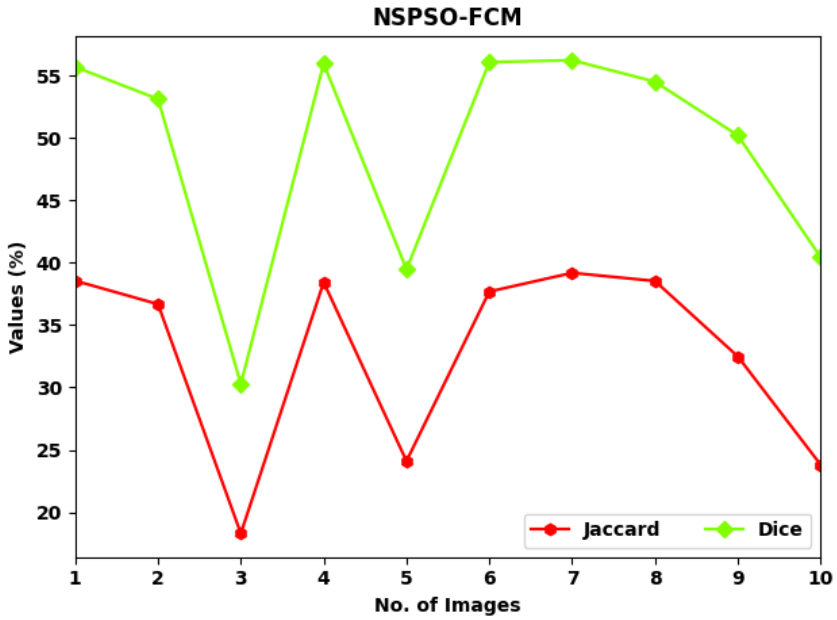

Fig. 4. Jaccard and Dice analysis of NSPSO-FCM Model

Fig. 5 portrays the results gotten by the FFCM model on ten distinct images. On applied image 1, the FFCM model has offered Jaccard and Dice of 34.14% and 49.84%. Similarly, on applied image 2, the FFCM model has provided Jaccard and Dice of 32.44% and 48.41%. Likewise, on applied image 3, the FFCM model has achieved Jaccard and Dice of 15.14% and 27.31%. Moreover, on applied image 4, the

DOI: https://doi.org/10.54216/IJNS.180202

Received: November 08, 2021 Accepted: March 02, 2022

FFCM model has attained Jaccard and Dice of 32.05% and 48.68%. Finally, on applied image 10, the FFCM model has resulted to Jaccard and Dice of 19.70% and 31.79%.

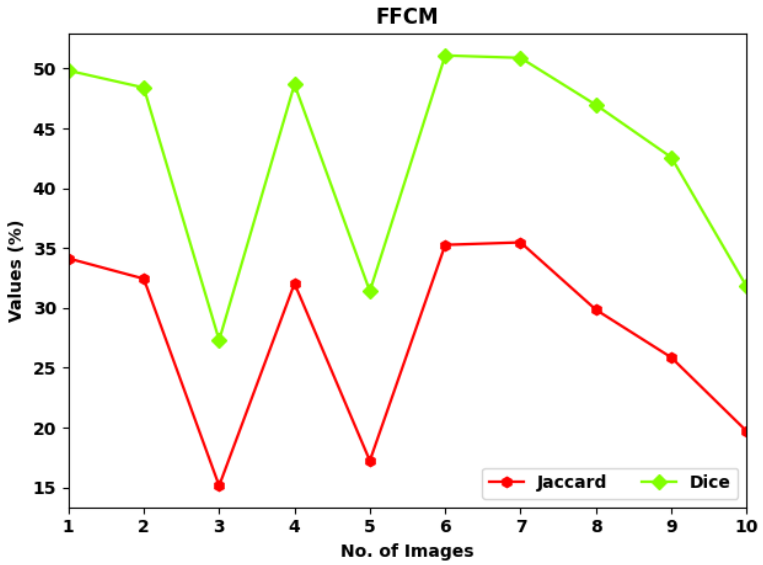

Fig. 5. Jaccard and Dice analysis of FFCM Model

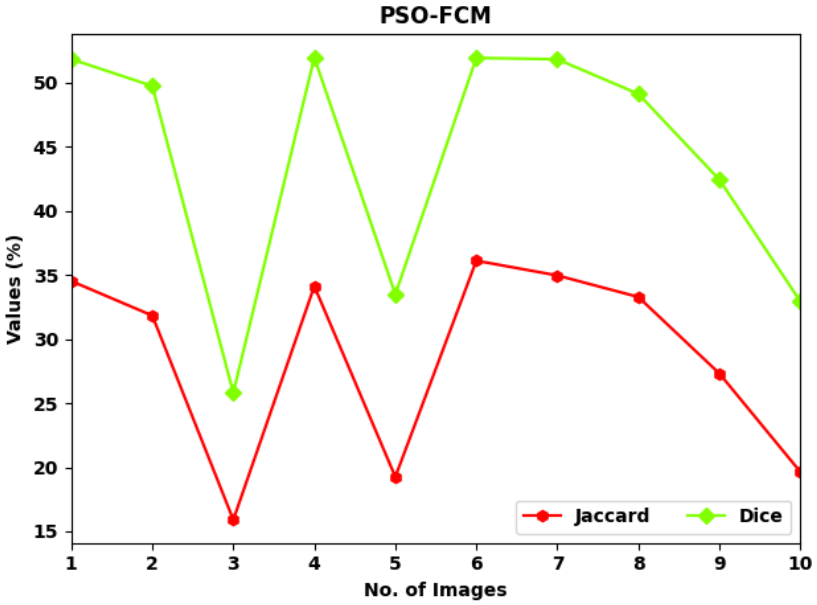

Fig. 6. Jaccard and Dice analysis of PSO-FCM Model

Fig. 6 shows the results gained by the PSO-FCM model on ten distinct images. On applied image 1, the PSO-FCM model has offered Jaccard and Dice of 34.53% and 51.85%. Similarly, on applied image 2, the PSO-FCM model has provided Jaccard and Dice of 31.84% and 49.76%. Likewise, on applied image 3, the PSO-FCM model has achieved Jaccard and Dice of 15.90% and 25.81%. Moreover, on applied image 4, the PSO-FCM model has attained Jaccard and Dice of 34.13% and 51.98%. Finally, on applied image 10, the PSO-FCM model has resulted to Jaccard and Dice of 19.64% and 32.94%.

DOI: https://doi.org/10.54216/IJNS.180202

Received: November 08, 2021 Accepted: March 02, 2022

Fig. 7 illustrates the results achieved by the NSANFIS-LTSC model on ten distinct images. On applied image 1, the NSANFIS-LTSC model has offered Jaccard and Dice of 42.11% and 58.44%. Similarly, on applied image 2, the NSANFIS-LTSC model has provided Jaccard and Dice of 40.59% and 56.13%. Likewise, on applied image 3, the NSANFIS-LTSC model has achieved Jaccard and Dice of 22.26% and 34.54%. Moreover, on applied image 4, the NSANFIS-LTSC model has attained Jaccard and Dice of 41.75% and 58.89%. Finally, on applied image 10, the NSANFIS-LTSC model has resulted to Jaccard and Dice of 27.88% and 43.58%.

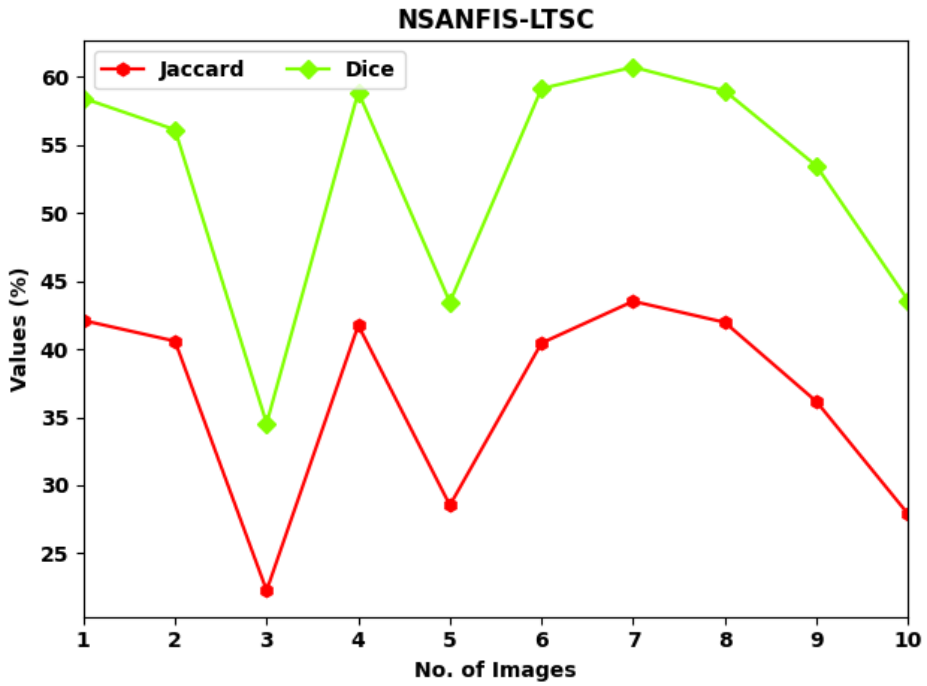

Fig. 7. Jaccard and Dice analysis of NSANFIS-LTSC model

Table 2 Comparative Jaccard Index analysis of NSANFIS-LTSC model

Jaccard Index (%)				
No. of Images	**NSPSO-FCM**	**FFCM**	**PSO-FCM**	**NSANFIS-LTSC**
Image-1	38.56	34.14	34.53	42.11
Image-2	36.68	32.44	31.84	40.59
Image-3	18.30	15.14	15.90	22.26
Image-4	38.44	32.05	34.13	41.75
Image-5	24.10	17.23	19.25	28.53
Image-6	37.69	35.27	36.12	40.45
Image-7	39.19	35.48	34.97	43.52
Image-8	38.54	29.85	33.29	41.97
Image-9	32.49	25.86	27.32	36.15
Image-10	23.81	19.70	19.64	27.88

Finally, a comparative Jacarrd index inspection of the NSANFIS-LTSC model with recent models in Table 2 and Fig. 8 [15]. The results indicated that the NSANFIS-LTSC model has accomplished higher Jaccard index values over the existing methodologies. For instance, with image 1, the NSANFIS-LTSC model has offered increased Jaccard index of 42.11% whereas the NSPSO-FCM, FFCM, and PSO-FCM

DOI: https://doi.org/10.54216/IJNS.180202

Received: November 08, 2021 Accepted: March 02, 2022

models have obtained lower Jaccard index of 38.56%, 34.14%, and 34.53%. Likewise, with image 2, the NSANFIS-LTSC model has offered increased Jaccard index of 40.59% whereas the NSPSO-FCM, FFCM, and PSO-FCM models have obtained lower Jaccard index of 36.68%, 32.44%, and 31.84%.

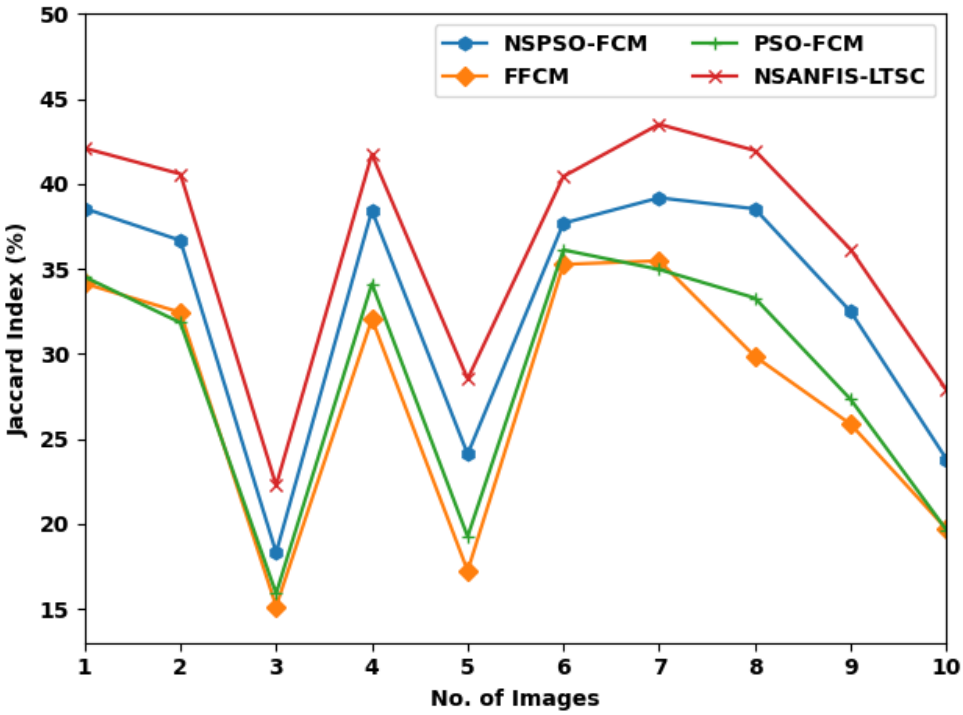

Fig. 8. Comparative results of NSANFIS-LTSC model with other models

Moreover, with image 7, the NSANFIS-LTSC model has offered increased Jaccard index of 43.52% whereas the NSPSO-FCM, FFCM, and PSO-FCM models have obtained lower Jaccard index of 39.19%, 35.48%, and 34.97%. After investigating the results using distinct images, it can be concluded that the NSANFIS-LTSC model has the ability of attaining superior liver tumor segmentation and classification performance.

4. Conclusion

This article has developed a new NSANFIS-LTSC to identify and classify the presence of liver tumor from medical images. The presented NSANFIS-LTSC model mainly undergoes pre-processing to eliminate the noise. In addition, NS based segmentation is applied to identify the affected tumor regions in the CT images. Moreover, DFA with DenseNet-169 model is utilized to create feature vectors and ANFIS classifier is exploited for the occurrence and classification of liver tumor. The simulation analysis of the NSANFIS-LTSC model is experimented using benchmark dataset and the results are investigated under several aspects. The simulation outcome reported the betterment of the NSANFIS-LTSC model over the recent methodologies interms of different measures. In future, deep instance segmentation models can be developed to improve the lung tumor classification results.

References

[1] Almotairi, S., Kareem, G., Aouf, M., Almutairi, B. and Salem, M.A.M., 2020. Liver tumor segmentation in CT scans using modified SegNet. Sensors, 20(5), p.1516.

[2] Rela, M., Suryakari, N.R. and Reddy, P.R., 2020, September. Liver tumor segmentation and classification: a systematic review. In 2020 IEEE-HYDCON (pp. 1-6). IEEE.

DOI: https://doi.org/10.54216/IJNS.180202

Received: November 08, 2021 Accepted: March 02, 2022

[3] Rezaei, M., Yang, H. and Meinel, C., 2018, July. Instance tumor segmentation using multitask convolutional neural network. In 2018 International Joint Conference on Neural Networks (IJCNN) (pp. 1-8). IEEE.
[4] Anter, A.M. and Hassenian, A.E., 2019. CT liver tumor segmentation hybrid approach using neutrosophic sets, fast fuzzy c-means and adaptive watershed algorithm. Artificial intelligence in medicine, 97, pp.105-117.
[5] Rao, C.S. and Karunakara, K., 2021. A comprehensive review on brain tumor segmentation and classification of MRI images. Multimedia Tools and Applications, 80(12), pp.17611-17643.
[6] Li, X., Chen, H., Qi, X., Dou, Q., Fu, C.W. and Heng, P.A., 2018. H-DenseUNet: hybrid densely connected UNet for liver and tumor segmentation from CT volumes. IEEE transactions on medical imaging, 37(12), pp.2663-2674.
[7] Rela, M., Nagaraja Rao, S. and Ramana Reddy, P., 2021. Optimized segmentation and classification for liver tumor segmentation and classification using opposition-based spotted hyena optimization. International Journal of Imaging Systems and Technology, 31(2), pp.627-656.
[8] Zhang, D., Chen, B., Chong, J. and Li, S., 2021. Weakly-supervised teacher-student network for liver tumor segmentation from non-enhanced images. Medical Image Analysis, 70, p.102005.
[9] Jiang, H., Diao, Z. and Yao, Y.D., 2021. Deep learning techniques for tumor segmentation: a review. The Journal of Supercomputing, pp.1-45.
[10] Anil, B.C. and Dayananda, P., 2021. Automatic liver tumor segmentation based on multi-level deep convolutional networks and fractal residual network. IETE Journal of Research, pp.1-9.
[11] Xu, Y., Cai, M., Lin, L., Zhang, Y., Hu, H., Peng, Z., Zhang, Q., Chen, Q., Mao, X., Iwamoto, Y. and Han, X.H., 2021. PA-ResSeg: A phase attention residual network for liver tumor segmentation from multiphase CT images. Medical Physics, 48(7), pp.3752-3766.
[12] Chlebus, G., Schenk, A., Moltz, J.H., van Ginneken, B., Hahn, H.K. and Meine, H., 2018. Automatic liver tumor segmentation in CT with fully convolutional neural networks and object-based postprocessing. Scientific reports, 8(1), pp.1-7.
[13] Deng, Z., Guo, Q. and Zhu, Z., 2019. Dynamic regulation of level set parameters using 3D convolutional neural network for liver tumor segmentation. Journal of healthcare engineering, 2019.
[14] Zheng, Z., Zhang, X., Xu, H., Liang, W., Zheng, S. and Shi, Y., 2018. A unified level set framework combining hybrid algorithms for liver and liver tumor segmentation in CT images. BioMed research international, 2018.
[15] Anter, A.M. and Hassenian, A.E., 2018. Computational intelligence optimization approach based on particle swarm optimizer and neutrosophic set for abdominal CT liver tumor segmentation. Journal of Computational Science, 25, pp.376-387.
[16] Zeng, M. and Xiao, N., 2019. Effective combination of DenseNet and BiLSTM for keyword spotting. IEEE Access, 7, pp.10767-10775.
[17] Mirjalili, S., 2016. Dragonfly algorithm: a new meta-heuristic optimization technique for solving single-objective, discrete, and multi-objective problems. Neural computing and applications, 27(4), pp.1053-1073.
[18] Thirumurugan, P. and Shanthakumar, P., 2016. Brain tumor detection and diagnosis using ANFIS classifier. International Journal of Imaging Systems and Technology, 26(2), pp.157-162.

DOI: https://doi.org/10.54216/IJNS.180202

Received: November 08, 2021 Accepted: March 02, 2022